Long-range correlations in the electric signals that precede rupture: Further investigations

P. A. Varotsos,[1,2,*] N. V. Sarlis,[1] and E. S. Skordas[1,2]
[1]*Solid State Section, Physics Department, University of Athens, Panepistimiopolis, Zografos, Athens 157 84, Greece*
[2]*Solid Earth Physics Institute, Physics Department, University of Athens, Panepistimiopolis, Zografos, Athens 157 84, Greece*
(Received 19 July 2002; revised manuscript received 25 October 2002; published 26 February 2003)

The correlations within the time series of the seismic electric signal (SES) activities have been studied in a previous paper [P. Varotsos, N. Sarlis, and E. Skordas, Phys. Rev. E **66**, 011902 (2002)]. Here, we analyze the time series of successive high- and low-level states' durations. The existence of correlation between the states is investigated by means of Hurst and detrended fluctuation analysis (DFA). The multifractal DFA (MF-DFA) is also employed. The results point to a stronger correlation, and hence longer memory, in the series of the high-level states. Furthermore, an analysis in the ''natural'' time domain reveals that certain power spectrum characteristics seem to distinguish SES activities from ''artificial'' (man-made) electric noises. More precisely, for natural frequencies $0<\phi<0.5$, the curves of the SES activities and artificial noises lie above and below, respectively, that of the ''uniform'' distribution (UD). A classification of these two types of electric signals (SES activities, artificial noises), cannot be achieved on the basis of the values of the power-law exponents alone, if the Hurst analysis, DFA, and MF-DFA are applied to the original time series. The latter two methods, however, seem to allow a distinction between the SES activities and artificial noises when treating them (not in conventional the time frame, but) in the natural time domain. To further test the techniques, a time series produced by another system was examined. We chose a signal of ion current fluctuations in membrane channels (ICFMCs). The following conclusions, among others, have been obtained: First, the power spectrum analysis in the natural time domain shows that the ICFMC curve almost coincides (in the range $0<\phi<0.5$) with that of the UD, and hence ICFMC lies just in the boundary between the SES activities and artificial noises. Second, MF-DFA indicates monofractality for the ICFMCs with a generalized Hurst exponent $h=0.84\pm0.03$ in the range 7–70 ms.

DOI: 10.1103/PhysRevE.67.021109 PACS number(s): 05.40.−a, 87.17.−d

I. INTRODUCTION

Seismic electric signals (SESs) are low frequency ($\leqslant 1$ Hz) changes of the electric field of the earth, which have been found in Greece [1–6] and Japan [7,8] to precede earthquakes with lead times ranging from several hours to a few months. It was suggested, long ago [9], that SES activities are emitted when a *critical* stress $\sigma=\sigma_{cr}$ is approached in the focal area. Actually, it has been recently found that the SES activities exhibit spectra that are consistent with those theoretically expected for critical phenomena [10,11]. This, however, can be only seen if we depart from the conventional time t by introducing instead [10] the natural time χ (see below). We clarify that, in an SES activity, Fig. 1(a), comprised of N pulses, χ is introduced by ascribing to the kth pulse the value $\chi_k=k/N$.

Beyond the SES activities, the continuously operating data collection system also records artificial noises, i.e., electrical disturbances due to nearby operating man-made sources. The discrimination between the SES activities and artificial noises is usually made by comparing their amplitudes recorded on a multitude of electric measuring dipoles (of various lengths ranging from a few tens of meters to several kilometers) and applying well known criteria (e.g., Ref. [2]). This can be significantly improved [4] if the time difference (arising from the *diffusing* nature [12] of the electromagnetic field, when transmitted in a conductive inhomogeneous medium such as the earth's crust) between the SES electrical variations and the associated magnetic field variations has been measured.

In a previous publication [13], using methods of statistical physics, we found that the SES activities exhibit long-range correlations (memory). Such long-range power-law correlations have been found in a wide variety of systems (e.g., see Ref. [14], and references therein). The quantiles procedure, introduced by Weron and co-workers (see Ref. [15], and references therein), was used for the study of the stationarity of the signal. The rescaled range Hurst analysis [16,17] and detrended fluctuation analysis (DFA) [18–20] led to power-law exponents that indicate long-range correlations. Furthermore, the natural time-domain analysis was applied to the SES activities as well as to the ion current fluctuations in membrane channels (ICFMCs). Within this frame, it was found [13] that certain power spectrum characteristics of the ICFMCs seem to distinguish them from the SES activities.

The analysis in the natural time domain was motivated by aspects of the theory of critical phenomena [10] (see also Ref. [13]) applied to the SES activities. Such an analysis naturally focuses on the long-range correlation between the high-level states (i.e., those having the largest deflections of the electric field amplitude with respect to the background level, low-level state). Instigated by this point, the present paper investigates, using various statistical methods, the correlations in the SES data (not only between successive electric field variations, but also) between the durations in each of the two states separately. Thus, the time series of subsequently high-level (T_h) and low-level (T_l) durations were

*Electronic address: pvaro@otenet.gr

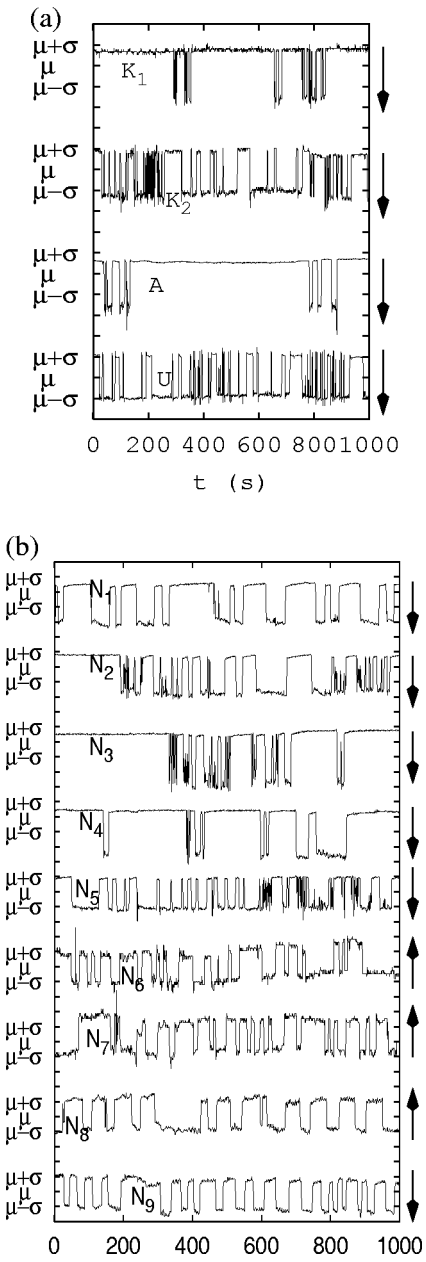

FIG. 1. Excerpts of (a) four SES activities labeled $K1$, $K2$, A, and U; (b) nine artificial noises labeled $N1$, $N2$, $N3$, $N4$, $N5$, $N6$, $N7$, $N8$, $N9$. In each case normalized units (dimensionless) were used, as described in Sec. II. The arrows to the right indicate the polarity of the deflection from the background level (i.e., from the low-level to the high-level states).

constructed $\{T_{h,j}\}_{j=1}^{N_h}$, $\{T_{l,j}\}_{j=1}^{N_l}$, where N_h and N_l $(=N_h-1)$ are the total number of the high- and low-level states' durations, respectively. We apply here the rescaled range Hurst [16,17], DFA [18–20], as well as the multifractal DFA [21] and the natural time-domain analysis [10,13]. The first two methods, between others, have been recently used [22] to study the time series of successive closed- and open-states' durations in the ICFMCs; they discovered that all techniques pointed to a stronger correlation in the series of closed states. We recall two points: First, single ionic channels in a membrane open and close spontaneously in a stochastic way, resulting in current and voltage changes, which resemble the realizations of random telegraph signals (RTSs) (dichotomous noise) (see Ref. [23], and references therein; see also Ref. [24]). The channel's opening state can be determined on the basis of the ion current: a low current corresponds to a closed channel state, while high-current values indicate an open state (e.g., see Ref. [25], and references therein). Second, the SES activities have also an RTS feature, which could be understood [9–11,26] in the context of dynamic phase transitions (critical phenomena).

The question of discriminating between a true signal (SES activity) and an artificial noise becomes a challenge when they look to be similar, although they are emitted from systems with different dynamics. It is one of the aims of this paper to attempt a plausible answer to this question, by taking advantage of the recently developed techniques in the time series analysis. This attempt includes the following steps: First, we investigate whether the original time series of the artificial noises exhibit long-range correlations (as already found for the other two types of electric signals, i.e., the SES activities and ICFMCs, which also have dichotomous nature). Second, we analyze for the artificial noises (in a similar fashion as explained above for the SES activities), the time series of each of the two states separately. We focus attention to the point whether a difference between the SES activities and artificial noises exists, when comparing the long-range correlations in the two states. In other words, this paper attempts to determine which correlations (i.e., those in the original time series or in the time series of the high- and low-levels' durations) differentiate between the SES activities and artificial noises.

The present paper is organized as follows: In Sec. II, we recapitulate a few experimental points related with the data sets of the electric signals analyzed in this paper. The Hurst analysis of the data is presented in Sec. III, while the results of both the DFA and the multifractal DFA (MF-DFA) are given in Sec. IV. In each of the latter two sections, we first present the analysis of the original time series and then proceed to the analyses of the series of the high- and low-levels states' durations. The results in each case are compared to those obtained for the ICFMCs. The spectrum analysis in the natural time domain is presented in Sec. V, while a short discussion of the results is given in Sec. VI. The main conclusions are summarized in Sec. VII. Two Appendixes are reserved as follows. Since the multifractal DFA method requires series of compact support, Appendix A presents a modification, called Euclidean (E-) approximation, which can be used to analyze data with fractal support. As for Appendix B, it provides an estimate of the errors introduced when we determine power-law exponents upon having to deal with small data sets.

II. EXPERIMENT

As examples, Fig. 1(a) depicts excerpts of four SES activities that preceded major earthquakes in Greece. The full records can be found in Refs. [3,4] for the SES activities labeled $K1$ and $K2$, in Ref. [5] for A, and in Ref. [6] for U (cf. only an excerpt of the SES activity $K1$ was shown in

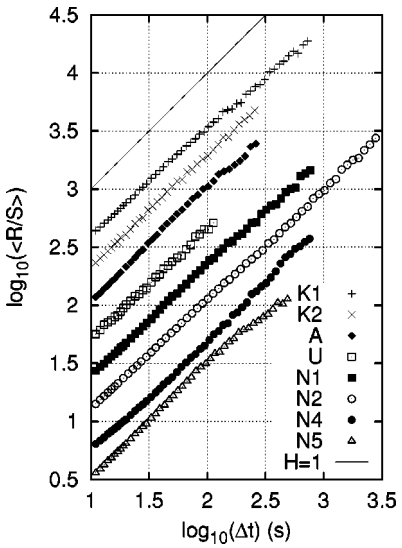

FIG. 2. The rescaled range analysis $\langle R/S\rangle$ as a function of Δt for the original time series of the SES activities and four (out of nine) artificial noises mentioned in Fig. 1.

Ref. [13]). Figure 1(b) shows a number of artificial noises that have been intentionally selected (among the multitude of noises that have several different shapes) to exhibit a (RTS) feature similar to that of the SES activities.

The SES activities and artificial noises shown in Fig. 1 were collected at various measuring sites. The electric field E is usually measured in mV/km, but here we present it in normalized units, i.e., by subtracting the mean value μ and dividing by the standard deviation σ. This will be called, hereafter, original time series in normalized units.

All the above signals have been collected with a sampling rate $f_{exp}=1$ sample/sec. Since the full record for the SES activities usually lasts for a time period of around a few hours, we usually deal with data sets consisting of $\approx 10^4$ data points. Thus, the series of high- and low-level states' durations have naturally a number of points one to two orders of magnitude less. Although the problem of treating short series has been discussed in the literature (e.g., Refs. [21,27]), we think it useful to offer the relevant estimates in Appendix B.

III. THE HURST ANALYSIS

The results of the so-called rescaled range analysis ($\langle R/S\rangle$), originated by Hurst [16], are given in Fig. 2 for the original time series of both the SES activities (the upper four curves) and four (out of nine) artificial noises mentioned in Fig. 1. (The results for all the cases mentioned in Fig. 1 are given in Ref. [28].) For the sake of convenience, the data points for each time series are vertically displaced after subsequent multiplication by a factor of 2, starting from $N5$; a continuous straight line corresponding to $H=1$ is also plotted. Since $\langle R/S\rangle(\Delta t)\sim(\Delta t)^H$, the value of the Hurst exponent H (labeled H_o in Table I) is found from the slope of the corresponding log-log plot, when approximating it with a single straight line.

An inspection of Fig. 2 and Table I shows that a value in the range $0<H<0.5$ (antipersistent time series, reflecting that increases in the values of a time series are likely to be followed by decreases, and conversely) cannot be seen. Furthermore, no case with $H=0.5$ (purely random changes) [9,29,30] can be recognized. In all the signals mentioned in Fig. 1 (see Table I), we find H_o values approximately between 0.9 and 1.0, which suggest the persistent character of the examined time series (long memory, e.g., see Refs.

TABLE I. Summary of the $\langle R/S\rangle$ analyses for all the signals mentioned in Fig. 1. H_o and H_d are the slopes determined by using the original time series and the dichotomous representation, respectively. H_{high} and H_{low} stand for the corresponding slopes for the high- and the low-level states' durations, respectively.

Signal	H_o	H_d	H_{high}	H_{low}
$K1$	0.90 ± 0.02	0.77 ± 0.04	0.85 ± 0.05	0.62 ± 0.05
$K2$	0.96 ± 0.01	0.81 ± 0.05	0.87 ± 0.09	0.70 ± 0.08
A	0.96 ± 0.02	0.76 ± 0.06	0.82 ± 0.28	0.61 ± 0.21
U	0.95 ± 0.02	0.80 ± 0.06	0.89 ± 0.13	0.72 ± 0.12
$N1$	0.94 ± 0.01	0.78 ± 0.05	0.70 ± 0.07	0.64 ± 0.06
$N2$	0.94 ± 0.01	0.84 ± 0.04	0.77 ± 0.03	0.58 ± 0.03
$N3$	0.97 ± 0.03	0.85 ± 0.04	0.80 ± 0.06	0.57 ± 0.05
$N4$	0.99 ± 0.03	0.87 ± 0.05	0.72 ± 0.04	0.63 ± 0.04
$N5$	0.94 ± 0.04	0.79 ± 0.06	0.76 ± 0.04	0.66 ± 0.04
$N6$	1.06 [a] ±0.02	0.86 ± 0.06	[b]	[b]
$N7$	0.93 ± 0.02	0.79 ± 0.05	[b]	[b]
$N8$	1.09 [a] ±0.02	0.86 ± 0.05	[b]	[b]
$N9$	1.01 [a] ±0.20	0.84 ± 0.25	0.75 ± 0.20	0.55 ± 0.22

[a]The value of H should not exceed unity (see the text), but here we reproduce the directly computed slope. Note that the computed H_d in the third column never exceeds unity.

[b]For $N6$, $N7$, and $N8$ no reliable slope could be determined in view of the small number of points ($N<25$).

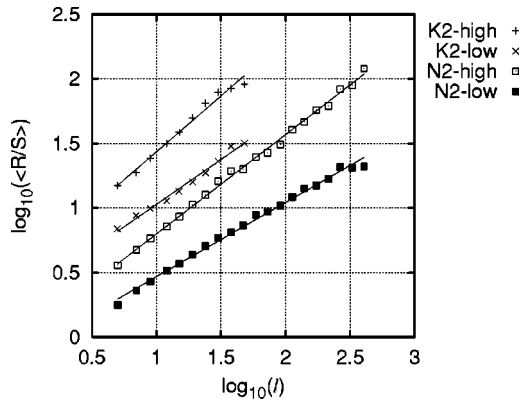

FIG. 3. The rescaled range analysis for the series of high- and low-level states' durations for an SES activity, $K2$, and an artificial noise, $N2$, mentioned in Fig. 1.

[15,17], and references therein). Note that if we repeat the analysis of Fig. 2, but for the dichotomous time series (i.e., converted from the original time series, ''0-1'' dichotomous representation), we find somewhat smaller values (labeled H_d in Table I), approximately in the range 0.75–0.90; the conclusion, however, for the persistent character of the time series still remains. In other words, this probably suggests that the long-range correlations in the time series examined, mainly arise from the dichotomous nature of the signals (see also Sec. VI concerning this point).

Recall that Mercik and Weron [15] reported for the ICFMCs a value $H=0.84\pm0.08$, which lies in the aforementioned range $H=0.75$–1.0 determined for the SES activities and artificial noises. Thus, when the Hurst analysis is carried out in the original time series (or in the corresponding dichotomous ones), the following conclusion emerges: Based on the values of the power-law exponents alone, no classification of the three type of signals, i.e., ICFMCs, SES activities, and artificial noises, can be achieved.

We now turn to the results of the Hurst analysis for the series of the high- and low-level states' durations. Two examples (one SES activity, i.e., $K2$, and one artificial noise, i.e., $N2$) are depicted in Fig. 3. The data points for each time series are vertically displaced after subsequent multiplication by a factor of 2, starting from the series of the low-level states' durations of $N2$. The results for all the cases mentioned in Fig. 1 can be found in Ref. [28]. The H values for all the cases are given in Table I, and reveal the following common characteristic for both the SES activities and artificial noises: The H values are systematically larger for the time series of the high-level states' durations (labeled H_{high}) when compared to the corresponding values (H_{low}) of the low-level ones. In spite of the large errors, the persistent character ($0.5<H<1$) of the series of the high-level states' durations seems to be well established; on the other hand, in view of the large estimation errors (due to the small number of points), we prefer not to draw any definite conclusion for the character of the series of the low-level ones (because several of the corresponding H_{low} values in Table I do not differ significantly from 0.5).

Hence, the long memory of the time series of both the SES activities and artificial noises may be mainly attributed to the strong correlation between the high-level states' durations. Note, however, that when comparing the SES activities and artificial noises, the H values of their high-level series (H_{high}) do not differ significantly enough (i.e., beyond the estimation errors) to guarantee any safe distinction between them. For the sake of comparison, we mention that for the ICFMCs, Siwy *et al.* [22] reported the values 0.67 ± 0.06 and 0.62 ± 0.06 for the series of the closed states and open states, respectively.

IV. CONVENTIONAL, MODIFIED, AND MULTIFRACTAL DETRENDED FLUCTUATION ANALYSIS

We start with a short description of the conventional DFA [18,19] (see also Ref. [31]). A thorough study of the extent to which fluctuation analysis can complement the classical power spectral analysis can be found in Ref. [32]. In summary, we first sum up the original time series and determine the profile $y(i), i=1,\ldots,N$; we then divide this profile of length N into N/l ($\equiv N_l$) nonoverlapping fragments of l-observations. Next, we define the detrended process $y_{l,\nu}(m)$, in the νth fragment, as the difference between the original value of the profile and the local (linear) trend. We then calculate the mean variance of the detrended process

$$F^2_{DFA}(l)=\frac{1}{N_l}\sum_{\nu=1}^{N_l}F^2(l,\nu), \tag{1}$$

where

$$F^2(l,\nu)=\frac{1}{l}\sum_{m=1}^{l}y^2_{l,\nu}(m). \tag{2}$$

Since $F_{DFA}(l)\sim l^{\alpha}$, the slope of the plot $\log[F_{DFA}(l)]$ versus $\log l$, leads to the value of the exponent α. In our case, since the time series is recorded with a frequency f_{exp}, we use the plot $\log[F_{DFA}(\Delta t)]$, because $\Delta t=l/f_{exp}$.

The above concerns the conventional DFA. The effect of the trends and noise on the DFA was later studied in detail by Hu *et al.* [20], while that of nonstationarities by Chen *et al.* [33]. Furthermore, Kantelhardt *et al.* [27], in order to improve the scaling of the DFA fluctuations on short scales l, suggested a modified fluctuation function

$$F_{mod}(l)=F_{DFA}(l)\frac{\langle[F^{shuff}_{DFA}(l')]^2\rangle^{0.5}l^{0.5}}{\langle[F^{shuff}_{DFA}(l)]^2\rangle^{0.5}l'^{0.5}}, \tag{3}$$

for $l'\gg l$, where $\langle[F^{shuff}_{DFA}(l')]^2\rangle^{0.5}$ denotes the DFA fluctuation function averaged over several configurations of shuffled data taken from the original record and $l'\approx N/20$. The improvement of such a modification was found very useful, especially for the short records of the high- and low-level states' durations analyzed in this paper (see also Appendix B).

A generalization of the DFA (hereafter called the MF-DFA) appeared recently in Ref. [21], and allows the multifractal characterization of nonstationary time series. In the MF-DFA, the following additional two steps should be made.

First, we average over all segments to obtain the qth-order fluctuation function

$$F_q(l) \equiv \left\{ \frac{1}{N_l} \sum_{\nu=1}^{N_l} [F^2(l,\nu)]^{q/2} \right\}^{1/q}, \tag{4}$$

where the index variable q can take any real value except zero. This is repeated for several scales l.

Second, we determine the scaling behavior of the fluctuation functions by analyzing log-log plots $F_q(l)$ versus l for each value of q. For long-range correlated series, $F_q(l)$ increases, for large values of l, as a power law: $F_q(l) \sim l^{h(q)}$, where the function $h(q)$ is called the generalized Hurst exponent. For stationary time series, $h(2)$ is identical [21] to the aforementioned Hurst exponent H. For monofractal time series, $h(q)$ is independent of q.

The improvement of Eq. (3) is useful to be incorporated into the MF-DFA as well [21]. Along these general lines, we multiplied $F_q(l)$ by an appropriate correction function to obtain

$$F'_q(l) = F_q(l) \frac{\langle F_q^{shuff}(l') \rangle l^{0.5}}{\langle F_q^{shuff}(l) \rangle l'^{0.5}}. \tag{5}$$

The MF-DFA method requires series of compact support. Here, in order to analyze data with fractal support, we followed a modification called Euclidean (E-) approximation described in Appendix A.

A. Results of the DFA

We start with the analysis of the original time series. Upon using the conventional DFA [31], we obtain the results depicted in Fig. 4 for both the SES activities and four (out of nine) artificial noises mentioned in Fig. 1. (The results for all the cases mentioned in Fig. 1 are given in Ref. [28].) The data points for each time series are vertically displaced after subsequent multiplication by a factor of 3, starting from $N5$. A least squares fit to a single straight line (despite the fact that the data, in some cases, obviously deviate from such a scheme, see below) reveals that the slopes of these log-log plots (labeled α_o in Table II) scatter, for all examples, around $\alpha \approx 1$, with a plausible uncertainty around 0.15. This reveals long-range correlations (as mentioned in Ref. [13] for the SES activities). If we repeat the analysis for the dichotomous time series, we find slightly different values for each case (labeled α_d in Table II), but the main conclusion (i.e., the strongly persistent character) remains the same. In other words, this suggests that the long-range correlations mainly arise from the dichotomous nature of the signals, as mentioned in Sec. III.

For the ICFMCs, if the DFA results are also described by a single straight line, a value $\alpha = 0.89 \pm 0.09$ is obtained [15]; this is more or less comparable with the value $\alpha \approx 1$ determined above for both SES activities and artificial noises. If the log-log plot in Fig. 4 is approximated with two straight lines, the following results are obtained: For both the SES activities and artificial noises (see Table II), the slope at shorter times [$\log_{10}(\Delta t)$ smaller than around 1.5, i.e., Δt approximately less than 30 s], labeled α_o^{short} in Table II, is found to lie approximately in the range $\alpha \approx 1.1$–1.4, while for longer times a value mostly in the range $\alpha \approx 0.8$–1.0 (labeled α_o^{long} in Table II) was determined, without, however, any safe classification between the SES activities and artificial noises on the basis of their α values alone. Applying the relation $\beta = 2\alpha - 1$ for the power spectrum exponent $S(f) \sim 1/f^{\beta}$, we find the values $\beta = 1.2$–1.8 and 0.6–1.0, respectively. For the ICFMCs, for times shorter than 70 ms, Siwy *et al.* [25] find $\alpha = 0.83 \pm 0.01$, while for longer times $\alpha = 1.04 \pm 0.04$.

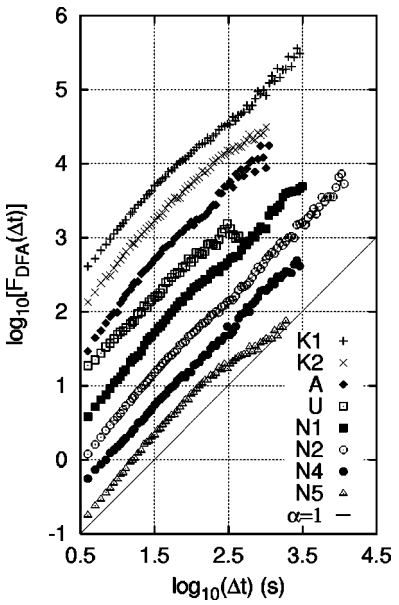

FIG. 4. The dependence of F_{DFA} on Δt in the conventional DFA of the original time series in normalized units of the SES activities and four (out of nine) artificial noises mentioned in Fig. 1. For the sake of convenience, a straight line corresponding to the slope $\alpha = 1$ is plotted.

We now proceed to the results for the series of the high- and low-level states' durations. In this analysis, we consider (see Appendix B) both the E approximation and the improvement of Eq. (5) for $q = 2$. Two examples, one SES activity ($K2$) and one artificial noise ($N2$) are depicted in Fig. 5; for the sake of clarity, the data points for the high- and low-level states' durations of $K2$ are vertically displaced after multiplying by 2 and 4, respectively. The results for all the cases mentioned in Fig. 1 are given in Ref. [28] and summarized in Table III. Three points emerge. First, a common characteristic for both the SES activities and artificial noises results: The α values for the series of the high-level states' durations are systematically larger than those of the series of the low-level ones (labeled α_{high} and α_{low}, respectively, in Table III). Second, the α values of the series of the high-level durations point to the following difference: For the SES activities, the α values lie approximately in the range 0.9–1.0 (cf. only for A, a somewhat smaller value $\alpha \approx 0.87$ is obtained, which might be due to an uncertainty of the calculation originating from the small number of points, see Appendix B), while for the artificial noises, they are markedly smaller, i.e., $\alpha \approx 0.65$–0.8 (cf. such a difference between the

TABLE II. Summary of the conventional DFAs for all the signals mentioned in Fig. 1. The symbols α_o and α_d stand for the DFA slopes obtained by using the original time series (in normalized units) and the dichotomous representation, respectively, for the whole Δt range. The corresponding slopes when considering, in each case, the range of either short Δt, smaller than $\approx$30s, or long Δt, larger than $\approx$30 s, are also shown.

Signal	α_o	α_o^{short}	α_o^{long}	α_d	α_d^{short}	α_d^{long}
$K1$	0.95 ± 0.04	1.19 ± 0.02	0.88 ± 0.02	0.95 ± 0.04	1.21 ± 0.04	0.90 ± 0.02
$K2$	0.95 ± 0.06	1.22 ± 0.04	0.81 ± 0.02	0.96 ± 0.06	1.23 ± 0.03	0.82 ± 0.02
A	1.06 ± 0.10	1.36 ± 0.05	0.96 ± 0.04	1.08 ± 0.10	1.41 ± 0.05	0.98 ± 0.04
U	0.95 ± 0.04	1.03 ± 0.05	0.81 ± 0.03	0.95 ± 0.04	1.07 ± 0.04	0.79 ± 0.03
$N1$	1.05 ± 0.05	1.26 ± 0.04	0.98 ± 0.02	1.01 ± 0.05	1.21 ± 0.04	0.95 ± 0.03
$N2$	1.04 ± 0.03	1.21 ± 0.03	1.01 ± 0.02	0.97 ± 0.03	1.12 ± 0.03	0.94 ± 0.02
$N3$	1.01 ± 0.04	1.15 ± 0.03	0.97 ± 0.02	0.99 ± 0.04	1.11 ± 0.03	0.95 ± 0.02
$N4$	1.04 ± 0.04	1.08 ± 0.03	1.02 ± 0.02	1.02 ± 0.04	1.01 ± 0.03	1.02 ± 0.02
$N5$	0.94 ± 0.10	1.22 ± 0.04	0.79 ± 0.02	0.92 ± 0.10	1.17 ± 0.04	0.78 ± 0.02
$N6$	1.14 ± 0.11	1.39 ± 0.04	0.89 ± 0.03	1.13 ± 0.11	1.43 ± 0.04	0.86 ± 0.03
$N7$	1.08 ± 0.09	1.32 ± 0.04	0.96 ± 0.03	1.03 ± 0.09	1.34 ± 0.04	0.82 ± 0.04
$N8$	1.15 ± 0.12	1.49 ± 0.04	0.78 ± 0.03	1.12 ± 0.12	1.45 ± 0.04	0.76 ± 0.03
$N9$	0.97 ± 0.20	1.53 ± 0.04	0.55 ± 0.02	0.93 ± 0.20	1.46 ± 0.04	0.52 ± 0.02

SES activities and artificial noises is not noticed, when comparing their series of the low-level states' durations). Third, comparing the α values between the series of the two-states' durations in the SES activities, we find that the α values of the series of the low-level states' durations (α_{low}) scatter around 0.5, thus being much smaller than the values $\alpha_{high} \approx 0.9$–$1.0$ for the series of the high-level states' durations.

For the sake of comparison, we now report the results of the DFA for the closed-states' and open states' durations of the ICFMCs. For the former series it was found [22]: that $\alpha=0.57\pm0.05$ for $l<70$ and 0.86 ± 0.07 for $l>70$, while for the latter $\alpha=0.62\pm0.06$ for all l. The value $\alpha=0.86$ in the closed-states' series, for large l, suggests the existence of strong long-range correlations. This result, along with other arguments [22], suggests that long-range correlations in the channel functioning are mainly due to the closed-states' memory.

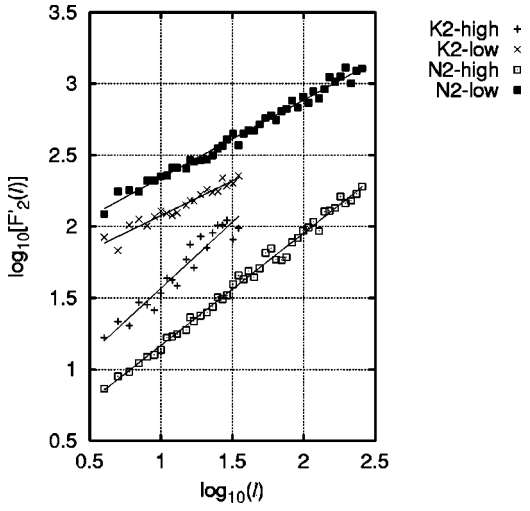

FIG. 5. The DFA analysis for the series of the high- and low-level states' durations [measured in seconds, and hence $F_2'(l)$ is also measured in seconds] for an SES activity and an artificial noise.

B. Results of the multifractal DFA

We draw attention to the following two points: First, following Ref. [21] we note that, when considering negative values of q, we focus on the segments with small fluctuations, which are usually described by a larger scaling exponent $h(q)$. For positive values of q, we focus on the segments with large fluctuations usually described by a smaller value of $h(q)$. Second, beyond the fact that we deal with short electrical records, these are practically continuously superimposed on variations induced by small changes of the earth's magnetic field [magnetotelluric (MT) variations]; such variations are expected to influence mainly our results on the segments of our electrical recordings with small fluctuations (cf. for time periods of intense MT variations, we have found a value $\alpha\approx2$, thus agreeing with the results of Fig. 4 of Hu *et al.* [20], when they studied sinusoidal functions with different amplitudes and periods T). In view of these two facts, we focus our discussion below on the q dependence of $h(q)$ for positive values of q only.

The results of the analysis of the original time series (in normalized units) for five examples, i.e., two SES activities ($K2$, A) and three artificial noises ($N2$, $N4$, $N5$), are depicted in Fig. 6 [the improvement of Eq. (5) was also considered]. The results for all the cases mentioned in Fig. 1 can be found in Ref. [28]. The q dependence of the asymptotic scaling exponent $h(q)$ was determined by fits to the log-log plots of $F_q'(l)$ vs l at the regimes where the fits are straight lines for all q. In view of the fact that a single straight line does not describe satisfactorily the experimental data in Fig. 4, the corresponding regimes were selected $K2$, $30\leqslant l \leqslant 1050$; A, $30\leqslant l\leqslant1125$; $N2$, $230\leqslant l\leqslant12000$, $N4$, $230\leqslant l \leqslant3200$, and $N5$, $230\leqslant l\leqslant2030$. An inspection of this figure shows that no obvious common characteristic can be recog-

TABLE III. Summary of the DFAs, by considering both the E approximation and the improvement of Eq. (5), for the series of the high- and low-level states' durations, along with the κ_1 values resulting from the power spectrum analysis in the natural time domain.

Signal	α_{high}	α_{low}	κ_1
$K1$	0.98 ± 0.08	0.31 ± 0.12	0.063 ± 0.003
$K2$	0.92 ± 0.10	0.49 ± 0.09	0.078 ± 0.004
A	0.87 ± 0.27	0.34 ± 0.25	0.068 ± 0.004
U	0.98 ± 0.13	0.70 ± 0.15	0.071 ± 0.004
$N1$	0.68 ± 0.07	0.70 ± 0.08	0.115 ± 0.003
$N2$	0.79 ± 0.03	0.54 ± 0.04	0.093 ± 0.003
$N3$	0.78 ± 0.06	0.47 ± 0.08	0.100 ± 0.008
$N4$	0.76 ± 0.06	0.55 ± 0.06	0.100 ± 0.013
$N5$	0.68 ± 0.05	0.62 ± 0.05	0.086 ± 0.007
$N6$	[a]	[a]	0.092 ± 0.004
$N7$	[a]	[a]	0.083 ± 0.006
$N8$	[a]	[a]	0.102 ± 0.004
$N9$	0.78 ± 0.20	0.11 ± 0.20	0.084 ± 0.004

[a]For $N6$, $N7$, and $N8$ no reliable slope could be determined in view of the small number of points ($N < 25$).

nized to allow any systematic distinction between the SES activities and artificial noises. In order to visualize the difficulty of such a distinction, we reproduce in the inset of Fig. 6, a case of an SES activity, i.e., A, which, when compared to the artificial noise $N4$, shows an almost identical dependence of $h(q)$ versus q (for $q<4$). The variation of $h(q)$ in the range $q \in (0,1]$ needs further investigation. We only note here that it is reminiscent of a scaling law, which relates different moments to one another, suggested in Ref. [34] to improve the quality of the estimates of the intermittency exponents in the analysis of energy cascade models of turbulence.

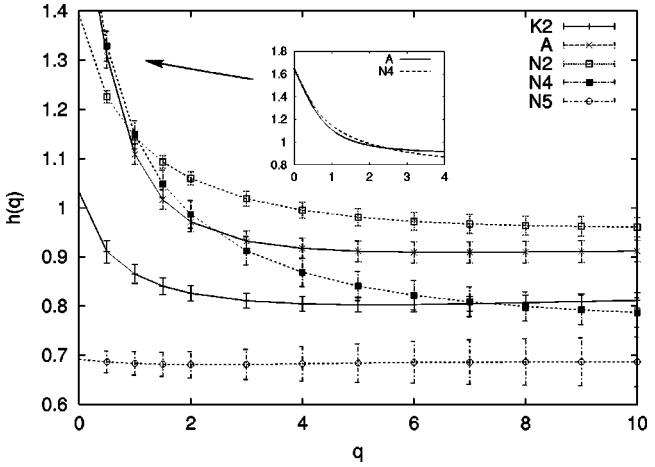

FIG. 6. The MF-DFA analysis for the original time series in normalized units of two SES activities (continuous curves) and three artificial noises (broken curves). The asymptotic standard error of the least-squares fit is also shown. In the inset, we intentionally reproduce an SES activity that exhibits $h(q)$ vs q dependence (for $q<4$) almost identical with an artificial noise.

When studying the series of the high- and low-level states' durations alone (examples are given in Fig. 7 for two SES activities, $K1$, $K2$, and two artificial noises, $N1$, $N2$, while the results for all the cases mentioned in Fig. 1 can be found in Ref. [28]), upon considering both the E approximation and the improvement of Eq. (5), a common feature emerges: In the time series of the high-level states (i.e., when MF-DFA is applied to the natural time domain), the $h(q)$ curves for the SES activities lie systematically higher (at least in the range $1.5 \leqslant q \leqslant 5$) than those in the case of artificial noises. For example, for $q=2$, the h values for the SES activities (i.e., α_{high} in Table III) lie close to unity, while for the artificial noises they scatter approximately in the range

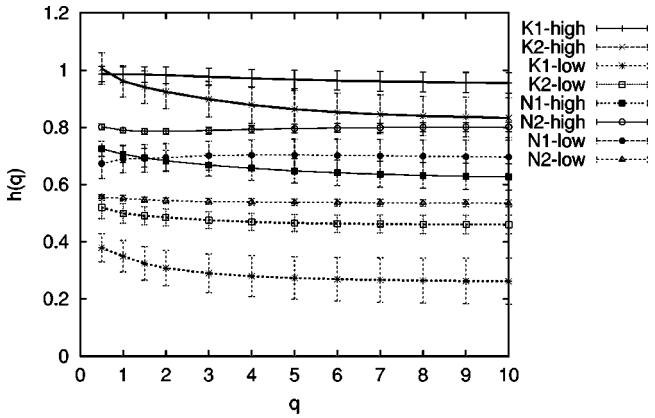

FIG. 7. The q dependence of the asymptotic scaling exponent $h(q)$ obtained from the MF-DFA analysis for the series of the high- and low-level states' durations (labeled high and low, respectively) for two SES activities (thicker lines) and two artificial noises (thinner lines). The former states (i.e., high-level) correspond to the continuous lines, while the latter to the dotted ones. The asymptotic standard error of the least-squares fit is also shown.

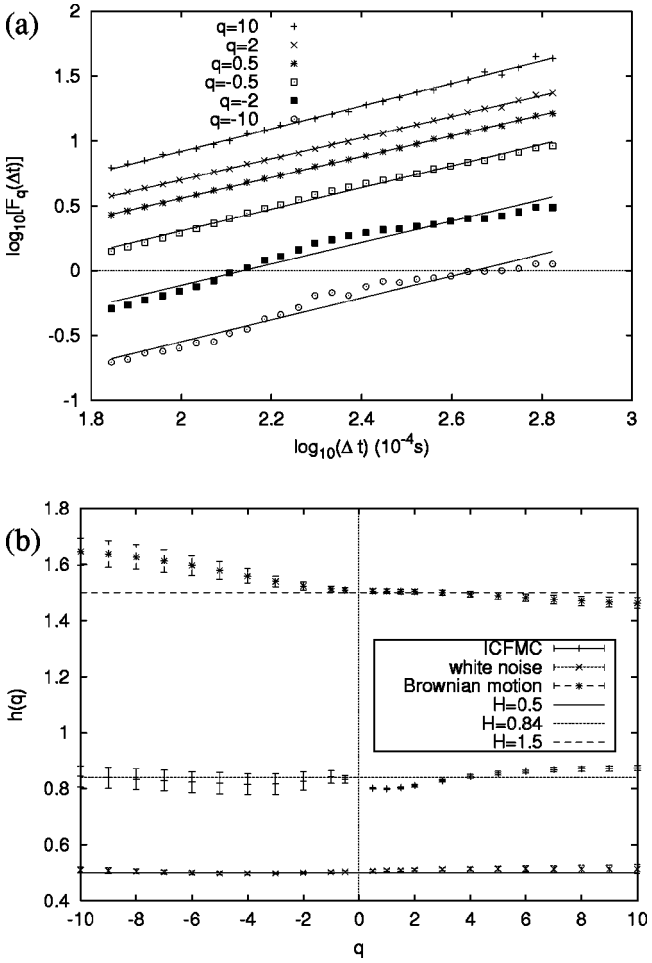

FIG. 8. The MF-DFA analysis, upon considering the *E* approximation, for the original time series in normalized units of the ICFMCs in the range 7–70 ms, i.e., 70–700 samples, $f_{exp}=10$ kHz. The asymptotic standard error of the least-squares fit is also shown in (b).

0.65–0.8. On the other hand, if we compare the series of the low-level states' durations (although, in general, they have smaller *h* values than those corresponding to the upper-level states' durations), no general feature can be recognized to discriminate the SES activities from the artificial noises.

We finally turn to the ICFMCs, and consider the MF-DFA of the original time series in the range $7-70$ ms. The q dependence of the asymptotic scaling exponent $h(q)$ depicted in Fig. 8(b) was determined by fits to the log-log plots of $F_q(\Delta t)$ versus Δt, shown in Fig. 8(a). For the sake of comparison, we give in Fig. 8(b) the corresponding q dependence of $h(q)$ calculated (using a single series of 40 000 data points, while the fits were made in the same range, i.e., 70–700 samples) for a white noise as well as for a Brownian motion. The present results for the ICFMCs indicate monofractality with $h=0.84\pm0.03$. (Recall that in the range below the crossover of 70 ms, Siwy *et al.* [25] determined a DFA exponent $\alpha=0.83\pm0.01$.) This fact essentially agrees with the suggestion of Mercik and Weron [15] that the relevant process can be identified with a fractional Brownian motion (FBM). The latter is the only Gaussian self-similar process with self-similarity index $H\neq0.5$.

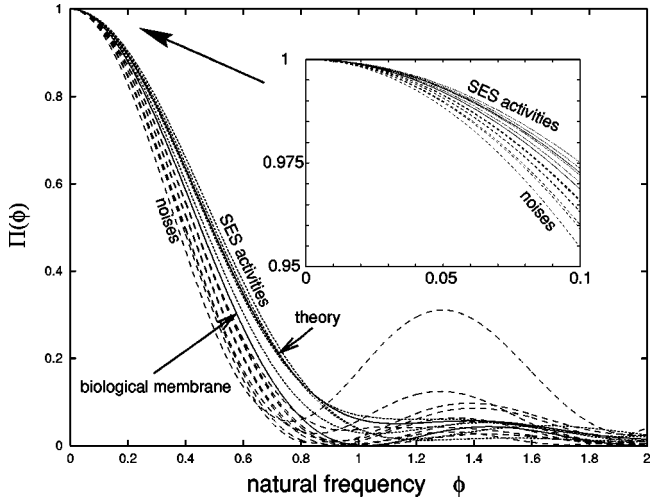

FIG. 9. The normalized power spectra $\Pi(\phi)$ for the SES activities (dotted lines) and the artificial noises (broken lines) mentioned in Fig. 1. The lower solid curve corresponds to the ICFMCs (labeled biological membrane), while the upper solid curve to the theoretical estimation of Eq. (8). For the sake of clarity, the curve corresponding to the "uniform" distribution was not drawn; this lies very close and only slightly below the the ICFMCs. The inset refers to the range $0\leqslant\phi\leqslant0.1$.

V. THE NATURAL TIME-DOMAIN ANALYSIS

We start with a short summary: Following Ref. [10] (see also Ref. [13]), we recall that the natural time χ serves as the index of an event (reduced by the total number of events). Let us, therefore, denote by Q_k the high-level state's duration of the kth pulse of an electric signal comprised of N pulses (Fig. 1). The natural time χ is introduced, as mentioned in the introduction, by ascribing to this pulse the value $\chi_k=k/N$. Considering the evolution (χ_k,Q_k), the continuous function $F(\omega)$ can be defined,

$$F(\omega)=\sum_{k=1}^{N}Q_k\exp\left(i\omega\frac{k}{N}\right), \tag{6}$$

where $\omega=2\pi\phi$, and ϕ stands for the *natural frequency*. We normalize $F(\omega)$ by dividing it by $F(0)$,

$$\Phi(\omega)=\frac{\sum_{k=1}^{N}Q_k\exp\left(i\omega\frac{k}{N}\right)}{\sum_{k=1}^{N}Q_k}=\sum_{k=1}^{N}p_k\exp\left(i\omega\frac{k}{N}\right), \tag{7}$$

where $p_k=Q_k/\Sigma_{n=1}^{N}Q_n$, and define the normalized power spectrum $\Pi(\omega)=|\Phi(\omega)|^2$. For natural frequencies ϕ less than 0.5, $\Pi(\omega)$ or $\Pi(\phi)$ reduces to a characteristic function for the probability distribution p_k in the context of probability theory. Examples of reading the SES activities in the natural time domain can be found in Refs. [10,11,13].

Figure 9 depicts the normalized power spectra, $\Pi(\phi)$, deduced from the analysis of both the SES activities and artificial noises mentioned in Fig. 1. The curves for the SES activities and artificial noises fall practically into two differ-

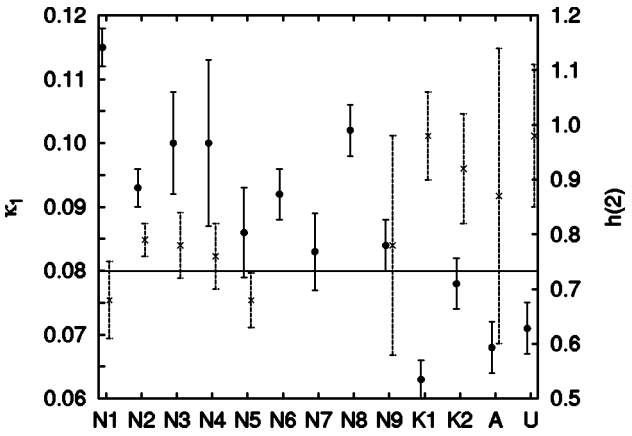

FIG. 10. Summary of the results of the analyses in the natural time domain. The results for the artificial noises $N1-N9$ and for the SES activities $K1$, $K2$, A, and U are depicted along with that for the ICFMCs (the latter corresponds to the solid horizontal line at $\kappa_1=0.080$). The solid circles correspond to the spectrum analysis (Sec. V) and are related with the κ_1 values (left vertical scale). The crosses correspond to the $h(2)$ values (right scale) obtained by the MF-DFA (Sec. IV). The SES activities scatter around the value $\kappa_1=0.070$ predicted from Eq. (8), and have $h(2)$ values that lie approximately in the range 0.87–1.0. The estimation errors are also shown.

ent classes, while the ICFMCs curve (when analyzed in the same frame, as mentioned in Ref. [13]) lies just between them. We now proceed to some comments on this classification. In the frame of dynamic phase transitions, by considering also the very stochastic nature of the relaxation process, the following relation was finally obtained in Ref. [10] (see also Ref. [13]):

$$\Pi(\omega)=\frac{18}{5\omega^2}-\frac{6\cos\omega}{5\omega^2}-\frac{12\sin\omega}{5\omega^3}. \tag{8}$$

For the region of natural frequencies $0<\phi<0.5$, the experimental results for the SES activities [10,11,13] (as well as that of the evolving seismicity, after the SES recording until each main shock, see Refs. [10,11,35]) scatter around the theoretical estimation of Eq. (8).

Expanding Eq. (8) around $\omega=0$, we get $\Pi(\omega)=1-0.07\omega^2+\cdots$. This implies [10,13] that the variance of χ is $\kappa_1=\langle\chi^2\rangle-\langle\chi\rangle^2=0.07$, which agrees with the κ_1 values obtained from the analysis of the SES activities (see the last column of Table III). The value of the variance κ_1 that reproduces artificial noises is larger than around 0.083, while for the ICFMCs data it was reported [13] to be 0.080 ± 0.003 (see also Fig. 10, where the error bars are also drawn). The fact that the ICFMCs lies just in the boundary between a ''universal'' curve obtained from the theory of critical phenomena (which agrees favorably with that of the SES activities) and the curves corresponding to fluctuations arising from man-made sources merits further investigation, see also the following section. Furthermore, we emphasize that the artificial noises, which are characterized by $\kappa_1\geqslant0.083$, are accompanied by $h(2)$ values, labeled α_{high} in Table III, smaller than ≈0.8 (see Fig. 10).

VI. DISCUSSION

The analysis presented in the previous sections shows a qualitative similarity of basic properties of the signals of dichotomous nature emitted, however, from three different systems, i.e., the SES activities, artificial noises, and the ICFMCs. Despite their quantitative differences related to the spatiotemporal scales of the investigated phenomena, they exhibit as a common characteristic the signature of scaling dynamics in complex systems. The existence of long-range correlations (under certain conditions) in time series of signals of dichotomous nature has been discussed in the literature. We now refer to two relevant efforts of developing mathematical tools on the study of *on-off* processes.

First, Willinger *et al.* [36] reported a key mathematical result concerning the *superposition* of many on-off sources with strictly alternating on and off periods and whose on periods or off periods have high variability (or infinite variance). They showed that the superposition of a large number of suitably scaled source-destination pairs, is approximately an FBM; this is an explanation of long-range dependence in a heavy tailed on-off process. An inspection of the results shows that only a number of artificial noises [i.e., the cases where $h(q)$ does not depend on q, for example, $N5$ in Fig. 6], could be identified as an FBM, while the SES activities time series do not.

Second, Heath *et al.* [37] constructed a stationary version of the on-off process of an *individual* source. Assuming heavy tailed (Pareto-like) long tails of the on and/or off periods, they showed that the on-off process of an individual source necessarily exhibits strong long-range dependence. This rigorous mathematical treatment, may provide the basis for the understanding of the power-law behavior of some artificial noises associated with individual sources. On the other hand, in the case of the SES activities, in view of the large volume of the earthquake preparation process (may be several tens of km^3) [38] and the existing inhomogeneities, a simultaneous achievement of the critical stress σ_{cr} at all points of the stressed volume should be probably excluded (see p. 419 of Ref. [9], i.e., the ''points'' obeying the condition $\sigma=\sigma_{cr}$ should lie on a ''surface'' that sweeps through the stressed volume). Thus, the description of the SES activity's emission on the basis of an individual source might not be appropriate.

The Hurst analysis and the DFA (Secs. III and IV) of the original time series of both the SES activities and artificial noises points to the existence of long-range correlations. Furthermore, an inspection of Tables I (compare the last two columns) and III (see the columns labeled α_{high} and α_{low}) suggests that the high-level states' durations of the SES activities exhibit drastically *stronger* memory than that of the low-level states' durations. We now proceed to an attempt towards understanding the results of the MF-DFA analysis (Sec. IV B), which show that the $h(2)$ values ($=H$) of the high-level states' durations of the SES activities (Fig. 7) are close to unity, while those of the artificial noises are mark-

edly smaller (see also Fig. 10). Let us consider, at the moment, for the sake of simplicity, the simple case of an FBM: the Hurst exponent H has been suggested as a measure of the *degree* (*intensity*) of self-similarity or long-range dependence [39,36]. [Willinger *et al.* [36] used the terms ''long-range dependence'' and ''(exactly or asymptotically second-order) self-similarity'' in an interchangeable fashion, because both refer to the tail behavior of the autocorrelations and are essentially equivalent. The power-law decay of the covariance characterizes long-range dependence. *The higher the H* the slower the decay.] If we now assume that, in general, $h(2)$ $(=H)$ is actually a measure of the intensity of long-range dependence, we may understand that the SES activities, since they exhibit *critical* dynamics (infinitely long-ranged interactions) should have a long-range dependence stronger (thus, a higher H) than that of the artificial noises. Note that the model [10,13] of critical behavior, which resulted in Eq. (8), shows that $\langle Q_k Q_{k+l} \rangle$ is independent of l.

We now turn to the discussion of the point that, when the signals are analyzed in the natural time domain, the ICFMCs curve in Fig. 9 seems to lie in the boundary between SES activities and artificial noises. In the limit of N tending to infinity, the distribution of p_k $(=Q_k/\Sigma_{n=1}^{N} Q_n)$ values will be substituted by a continuous function $p(\chi)$, for $\chi \in (0,1]$. In this region, $p(\chi)$ can be expanded in a cosine Fourier series $p(\chi)=1+\Sigma_{n=1}^{\infty} \mathrm{p}_n \cos(n\pi\chi)$ where $\mathrm{p}_n = 2\int_0^1 p(\chi)\cos(n\pi\chi)d\chi$, are the Fourier expansion coefficients. One can show that the following interrelation [10]

$$\kappa_1 = \langle \chi^2 \rangle - \langle \chi \rangle^2 = \frac{1}{12} + \frac{1}{2\pi^2} \sum_{k=1}^{\infty} \frac{\mathrm{p}_{2k}}{k^2} - \left[\frac{1}{2\pi^2} \sum_{k=0}^{\infty} \frac{\mathrm{p}_{2k+1}}{(k+1/2)^2} \right]^2 \quad (9)$$

is found between κ_1 and p_k (recall that the various normalized power spectra in Fig. 9 are grouped together as ω or ϕ tend to 0 according to their κ_1 values, see the Appendix of Ref. [13]). This relation shows that if we assume a uniform distribution, i.e., all p_k tend to zero, we find that $\kappa_u = 1/12 \approx 0.083$, where the subscript u stands for the uniform distribution; the latter corresponds to a curve located very close to, and only slightly below (and hence, for the sake of clarity, not drawn in Fig. 9) the one labeled ''biological membrane'' in Fig. 9. We now recall, from Sec. V, that for the SES activities $\kappa_1 \approx 0.070$, while for the artificial noises $\kappa_1 \geqslant 0.083$. If it is justified to assume that the quantity $\langle \chi^2 \rangle - \langle \chi \rangle^2$ $(=\kappa_1)$ provides a measure [10] of the ''average uncertainty'' of the evolution of the dynamic system under discussion, we may say the following: when compared to a uniform distribution, the SES activities and artificial noises have smaller and larger average uncertainty, respectively. (This is not unreasonable, if we recall that the SES activities—critical dynamics, see the previous paragraph—have stronger long-range correlations than the artificial noises in their high-level states' durations, i.e., in the natural time domain.) Thus, it may be understood that the curves of the SES activities and artificial noises lie in Fig. 9 above and below the curve of the uniform distribution, respectively. The fact that the ICFMCs curve $(\kappa_1 = 0.080 \pm 0.003)$ lies between the curves of the SES activities and artificial noises in Fig. 9 may reflect that the ICFMCs lies closer to the ''uniform'' distribution, compared either to the SES activites or the (majority of the) artificial noises, which is not unreasonable for such a biological system.

Finally, we comment on the very pronounced ''modes'' in some artificial noises depicted in Fig. 9. Their exact origin cannot be identified with certainty; they probably reflect that the corresponding artificial sources cannot be related with the critical phenomena formalism (recall that the latter is represented by the solid curve labeled theory in the same figure, and does not show any such pronounced mode).

VII. CONCLUSIONS

Long-range correlations (memory) do exist in all the three types of electric signals investigated, i.e., the ICFMCs, the SES activities, and artificial (man-made) noises. The results of the analyses suggest that the strong memory of the SES activities is mainly (if not solely) due to the high-level states. This, in reality, justifies the suggestion of the concept of natural time, which was motivated on different grounds. Furthermore, it is reminiscent of the recent result [22] that the series of the closed-states' durations of the ICFMCs have a longer memory than the open ones (recall, however, that the closed states refer to low-current values, while the open to high-current). Upon using various statistical methods (Hurst, DFA, multifractal DFA, and spectrum analysis in the natural time domain), the following specific conclusions could be also drawn.

First, when approximating the log-log plot with a single straight line, the use of either the Hurst analysis or the DFA in the original time series leads to comparable values of the corresponding power-law exponents for all the three types of electric signals investigated. Furthermore, the application of the multifractal DFA to the original time series cannot discriminate between the SES activities and artificial noises. For the ICFMCs, and in the region 7–70 ms, the MF-DFA indicates monofractality with $h = 0.84 \pm 0.03$.

Second, the DFA as well as the multifractal DFA seem to provide a distinction between the SES activities and artificial noises, but *only* if the analysis is made for the series of the high-level states' durations. This, in reality, means that the relevant tools are handled in the natural time domain [see Fig. 10, where the SES activities are clustered around the ''region'' having $\kappa_1 \approx 0.070$ and $h(2)$ values close to unity].

Third, the spectrum analysis in the natural time domain seems to allow a classification of the three types of signals, the ICFMCs, the SES activities, and artificial noises. More precisely, the latter two types of signals can be distinguished as follows: for natural frequencies $0 < \phi < 0.5$, the SES activities fall practically on a universal curve which coincides to that expected from concepts of critical phenomena [13], while the artificial noises belong to a different class of curves. The artificial noises have a variance κ_1, larger than around $\kappa_1 = 0.083$, which is markedly higher than that, i.e., $\kappa_1 = 0.070$, associated with the SES activities, see Fig. 10. Furthermore, it seems that certain power spectrum characteristics of the ICFMCs lie *just in the boundary* (Fig. 9) be-

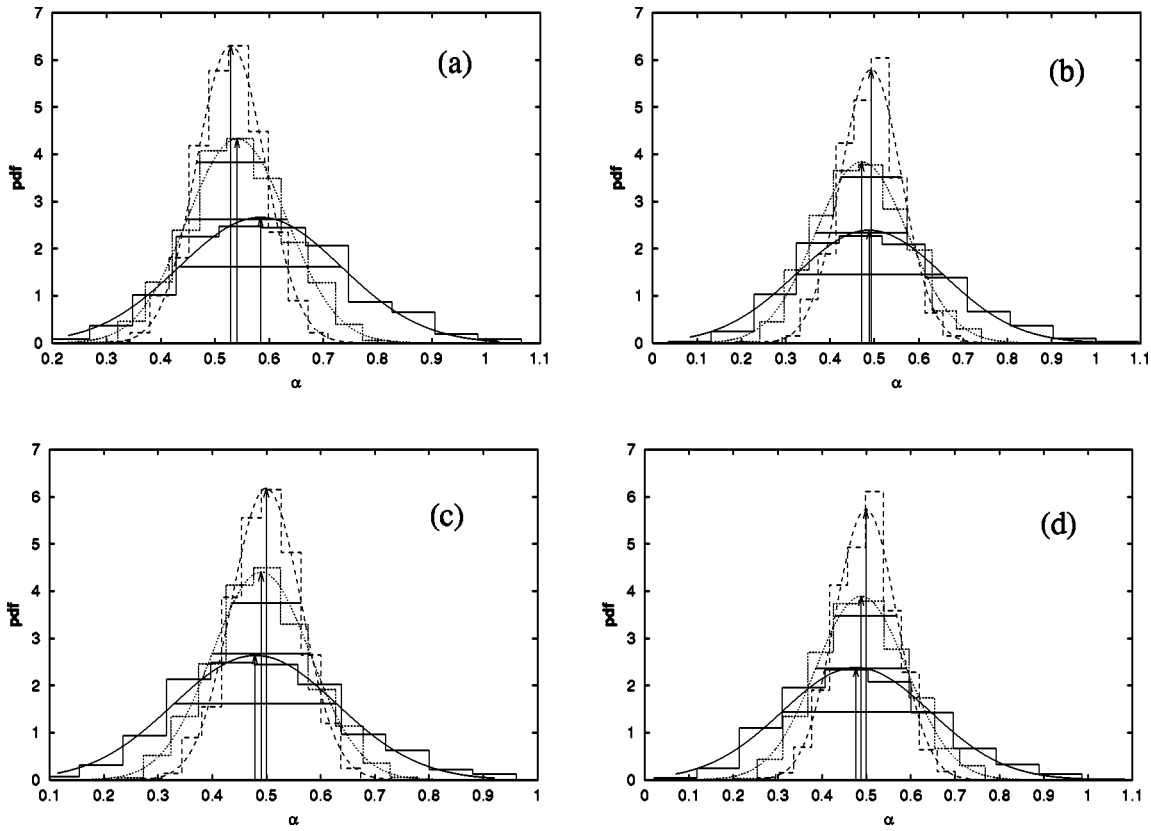

FIG. 11. Histograms of α, calculated by 1000 realizations of Gaussian noise ($H=0.5$) using various versions of the DFA: (a) conventional DFA, (b) DFA with E approximation, (c) DFA with the improvement of Eq. (5) for $q=2$, and (d) a DFA which considers both, i.e., E approximation and the improvement of Eq. (5) for $q=2$. The results are shown for time series of lengths $N=50$ (solid lines), 100 (dotted lines), 200 (broken lines) along with the corresponding Gaussian fits. The positions of the mean and the region of one standard deviation are shown by the vertical arrows and horizontal solid lines in each case, respectively.

tween the SES activities and artificial noises. This might be understood in the following context: the ICFMCs curve almost coincides with (lying only slightly above) that of the uniform distribution (UD, as it was defined in Sec. VI, which has a variance $\kappa_u=0.0833\ldots$), as intuitively expected for this system. On the other hand, the curves of the SES activities ($\kappa_1\approx 0.070$) and the artificial noises ($\kappa_1\geqslant 0.083$) lie above and below, respectively, the curve of UD.

In other words, the key point which differentiates SES activities from artificial noises is the fact that the memory of the high-level states in the SES activities is drastically stronger than that of the low-level states. As for the difference between the memory of the two states in the ICFMCs, it is not so large as that found in the SES activities (critical dynamics).

ACKNOWLEDGMENTS

We express our sincere thanks to Professor K. Weron and Dr. S. Mercik for fruitful suggestions as well as for sending us a lot of useful information on their work. We also thank Professor P. N. R. Usherwood and Dr. I. Mellor for providing us with the experimental data of ion current through a high conductance locust potential channel. Stimulating discussions with Professor E. Manousakis are gratefully acknowledged. We also thank Professor Dr. Peter Talkner who called our attention to Ref. [40], which had suggested the generalization of the DFA to a multifractal method.

APPENDIX A: THE EUCLIDEAN (E) APPROXIMATION FOR MF-DFA

The MF-DFA method requires series of compact support. In order to analyze data with fractal support, the following modification was suggested in Ref. [21]: The sum in Eq. (4) is restricted to the local maxima, i.e, to those terms $F^2(l,\nu)$ that are larger than the terms $F^2(l,\nu-1)$ and $F^2(l,\nu+1)$ for the neighboring segments. By this restriction all terms $F^2(l,\nu)$ that are zero or very close to zero will be disregarded, and series with fractal support can be analyzed. Towards this goal, we follow in this paper a slightly different modification, which for reasons of brevity, will be called the Euclidean (E) approximation. In this approximation, instead of $[F^2(l,\nu)]^{q/2}$, the Euclidean "distance" $d(l,\nu)\equiv([F^2(l,\nu-1)]^q+[F^2(l,\nu)]^q+[F^2(l,\nu+1)]^q)^{1/2}$ is used. In a simple geometrical picture, if we assume that $d_1=[F^2(l,\nu-1)]^{q/2}$, $d_2=[F^2(l,\nu)]^{q/2}$, and $d_3=[F^2(l,\nu+1)]^{q/2}$ represent displacements (parallel to each of the three axes of a Cartesian system) that form a path, the Euclidean distance

$d(l,\nu)=\sqrt{d_1^2+d_2^2+d_3^2}$ lies between the total length $d_1+d_2+d_3$ of the path and any of its side lengths, i.e., $d_1,d_2,d_3 \leqslant d(l,\nu) \leqslant d_1+d_2+d_3$; thus

$$\{\max[F^2(l,\nu-1),F^2(l,\nu),F^2(l,\nu+1)]\}^{q/2} \leqslant d(l,\nu) \leqslant [F^2(l,\nu-1)]^{q/2}+[F^2(l,\nu)]^{q/2}+[F^2(l,\nu+1)]^{q/2}. \tag{A1}$$

If we consider the above inequality and perform the summation over ν in the definition of the qth-order fluctuation function of Eq. (4), we deduce that the E approximation lies between the aforementioned local maxima modification [21] and the usual MF-DFA method (the latter being multiplied by factor of ≈ 3). In order to verify whether the E approximation works correctly from statistical point of view, we performed the calculations presented in Appendix B, which show that it improves the conventional DFA for small N. The E approximation is reminiscent of the replacement of the maximum norm, used in Ref. [41], by the Euclidean norm in the estimation [42] of the (lower bound of the) Kolmogorov-Sinai invariant (entropy) (see also p. 649 of Ref. [43]).

APPENDIX B: EXPONENTS DETERMINED BY THE DFA FOR SHORT SERIES

When analyzing an SES activity in the conventional time frame, as mentioned in Sec. II, the length of the series is of the order of 10^4. However, this length may decrease down to 10^2 when studying the series of the high- and low-states' durations. A question therefore naturally arises on how large are the statistical and systematic errors of exponents, practically determined by the DFA for such short series, where the statistics is expected to be poor. In an attempt to address this question, Gaussian noise time series ($H=0.5$) of lengths $N=50$, 100, and 200 were generated, and the exponents α for 1000 such series were calculated. In each case, four versions of the DFA have been used. Figure 11 shows the results: conventional [31] DFA, Fig. 11(a), DFA with E approximation, Fig. 11(b), DFA using the improvement of Eq. (5), Fig. 11(c), and a DFA which considers both the E approximation and the improvement of Eq. (5), Fig. 11(d). This figure indicates that the statistical errors (the standard deviation of the Gaussian fits to the histograms) practically depend on the size of the series only. They do not vary significantly from version to version, and have values ≈ 0.16, 0.10, and 0.07 for $N=50$, 100, and 200, respectively. On the other hand, there are systematic errors in the conventional DFA for small N, which can be almost removed upon using, either the improvement of Eq. (5), or the E approximation, or both. These systematic errors decrease, as expected, with increasing N, for all methods, resulting in an ''optimum''; this considers both Eq. (5) as well as the E approximation, and accounts for ''shuffling'' and ''no-compactness,'' respectively. It is noteworthy, however, that for small sample sizes, although the systematic error can be essentially eliminated, the statistical error does remain and should be always carefully considered (this was actually followed in Table III).

[1] P. Varotsos, K. Alexopoulos, K. Nomicos, and M. Lazaridou, Nature (London) **322**, 120 (1986).

[2] P. Varotsos and M. Lazaridou, Tectonophysics **188**, 321 (1991).

[3] P. Varotsos, M. Lazaridou, K. Eftaxias, G. Antonopoulos, J. Makris, and J. Kopanas, in *The Critical Review of VAN: Earthquake Prediction from Seismic Electric Signals*, edited by S. J. Lighthill (World Scientific, Singapore, 1996), p. 29.

[4] P. Varotsos, N. Sarlis, and E. Skordas, Proc. Jpn. Acad., Ser. B: Phys. Biol. Sci. **77**, 93 (2001).

[5] P. Varotsos, N. Sarlis, and E. Skordas, Acta Geophys. Pol. **49**, 425 (2001).

[6] P. Varotsos, N. Sarlis, E. Skordas, and M. Lazaridou, Practica Athens Acad. **77**, 111 (2002).

[7] S. Uyeda, T. Nagao, Y. Orihara, T. Yamaguchi, and I. Takahashi, Proc. Natl. Acad. Sci. U.S.A. **97**, 4561 (2000).

[8] S. Uyeda, M. Hayakawa, T. Nagao, O. Molchanov, K. Hattori, Y. Orihara, K. Gotoh, Y. Akinaga, and H. Tanaka, Proc. Natl. Acad. Sci. U.S.A. **99**, 7352 (2002).

[9] P. Varotsos and K. Alexopoulos, *Thermodynamics of Point Defects and their Relation with Bulk Properties* (North-Holland, Amsterdam, 1986).

[10] P. Varotsos, N. Sarlis, and E. Skordas, Practica Athens Acad. **76**, 388 (2001).

[11] P. Varotsos, *The Physics of Seismic Electric Signals* (Terrapub, Tokyo, in press).

[12] P. Varotsos, N. Sarlis, and M. Lazaridou, Phys. Rev. B **59**, 24 (1999).

[13] P.A. Varotsos, N.V. Sarlis, and E.S. Skordas, Phys. Rev. E **66**, 011902 (2002).

[14] H.E. Stanley, Rev. Mod. Phys. **71**, S358 (1999).

[15] S. Mercik and K. Weron, Phys. Rev. E **63**, 051910 (2001).

[16] H.E. Hurst, Trans. Am. Soc. Civ. Eng. **116**, 770 (1951).

[17] J. Bassingthwaighte, L.S. Liebovitch, and B.J. West, *Fractal Physiology* (Oxford University Press, Oxford, 1994).

[18] C.-K. Peng, S.V. Buldyrev, S. Havlin, M. Simons, H.E. Stanley, and A.L. Goldberger, Phys. Rev. E **49**, 1685 (1994).

[19] S.V. Buldyrev, A.L. Goldberger, S. Havlin, R.N. Mantegna, M.E. Matsa, C.-K. Peng, M. Simons, and H.E. Stanley, Phys. Rev. E **51**, 5084 (1995).

[20] K. Hu, P.C. Ivanov, Z. Chen, P. Carpena, and H.E. Stanley, Phys. Rev. E **64**, 011114 (2001).

[21] J. Kantelhardt, S.A. Zschiegner, E. Koscielny-Bunde, A. Bunde, S. Havlin, and H.E. Stanley, e-print physics/0202070.

[22] Z. Siwy, S. Mercik, K. Weron, and M. Ausloos, Physica A **297**, 79 (2001).

[23] A. Fuliński, Z. Grzywna, I. Mellor, Z. Siwy, and P.N.R. Usherwood, Phys. Rev. E **58**, 919 (1998).

[24] S. Mercik, K. Weron, and Z. Siwy, Phys. Rev. E **60**, 7343 (1999).

[25] Z. Siwy, M. Ausloos, and K. Ivanova, Phys. Rev. E **65**, 031907 (2002).

[26] P. Varotsos, Acta Geophys. Pol. **49**, 1 (2001).
[27] J. Kantelhardt, E. Koscielny-Bunde, H. Rego, S. Havlin, and A. Bunde, Physica A **295**, 441 (2001).
[28] See EPAPS Document No. E-PLEEE8-67-110302 for the analysis of the totality of cases mentioned in Fig. 1. A direct link to this document may be found in the online article's HTML reference section. The document may also be reached via the EPAPS homepage (http://www.aip.org/pubservs/epaps.html) or from ftp.aip.org in the directory/epaps/. See the EPAPS homepage for more information.
[29] G.H. Weiss, *Random Walks* (North-Holland, Amsterdam, 1994).
[30] G.H. Weiss, Physica A **311**, 381 (2002).
[31] See A.L. Goldberger, L.A.N. Amaral, L. Glass, J.M. Hausdorff, P.C. Ivanov, R.G. Mark, J.E. Mietus, G.B. Moody, C.-K. Peng, and H.E. Stanley, Physionet, http://circ.ahajournals.org/cgi/content/full/101/23/e215.
[32] P. Talkner and R.O. Weber, Phys. Rev. E **62**, 150 (2000).
[33] Z. Chen, P.C. Ivanov, K. Hu, and H.E. Stanley, Phys. Rev. E **65**, 041107 (2001).
[34] R. Badii and P. Talkner, Phys. Rev. E **59**, 6715 (1999).
[35] P. Varotsos, N. Sarlis, and E. Skordas, Acta Geophys. Pol. **50**, 337 (2002).
[36] W. Willinger, M.S. Taqqu, R. Sherman, and D.V. Wilson, IEEE ACM Trans. Networking **5**, 71 (1997).
[37] D. Heath, S. Resnick, and G. Samorodnitsky, Math. Op. Res. **23**, 145 (1998).
[38] P. Varotsos, N. Sarlis, M. Lazaridou, and P. Kapiris, J. Appl. Phys. **83**, 60 (1998).
[39] M.S. Taqqu, V. Teverovsky, and W. Willinger, Fractals **3**, 785 (1995).
[40] R. Weber and P. Talkner, J. Geophys. Res., [Atmos.] **106**, 20131 (2001).
[41] F. Takens, in *Atas do 13. Coloquio Brasiliero de Matematica*, edited by IMPA (IMPA, Rio de Janeiro, 1983).
[42] P. Grassberger and I. Procaccia, Phys. Rev. A **28**, 2591 (1983).
[43] J.-P. Eckmann and D. Ruelle, Rev. Mod. Phys. **57**, 617 (1985).